Available online at www.sciencedirect.com

SciVerse ScienceDirect

Journal of the European Ceramic Society 32 (2012) 975–987

www.elsevier.com/locate/jeurceramsoc

Development of a black ceramic pigment from non stoichiometric hydrotalcites

V. Rives [a,*], M.E. Pérez-Bernal [a], R.J. Ruano-Casero [a], I. Nebot-Díaz [b]

[a] GIR-QUESCAT, Departamento de Química Inorgánica, Universidad de Salamanca, 37008 Salamanca, Spain
[b] Escola Superior de Cerámica de L'Alcora. Av. Corts Valencianes, 23, L'Alcora, 12110 Castellón, Spain

Received 7 July 2011; received in revised form 10 November 2011; accepted 22 November 2011
Available online 16 December 2011

Abstract

Non stoichiometric layered double hydroxides (LDHs) with the hydrotalcite-like structure and containing Co^{2+} and Cr^{3+} cations in the brucite-like layers have been prepared by coprecipitation at room temperature from aqueous solutions of the corresponding chlorides. Five samples have been prepared, with Co/Cr molar ratios ranging from 2/1 to 1/2. The solids have been characterised by element chemical analysis for cations, powder X-ray diffraction, differential thermal analysis, thermogravimetric analysis, temperature-programmed reduction, Fourier transform-infrared and visible–ultraviolet spectroscopies, and particle size and specific surface area determination. The colorimetric parameters have been also measured. Their calcination at high temperature to yield homogeneously mixed metal oxides has been carried out. Both the original and the calcined solids have been dispersed in two enamels and the colorimetric parameters have been determined too. The optimum composition to yield a black pigment (bulk or dispersed in colourless or white enamels) has been determined.

Keywords: Powders-chemical preparation; Microstructure-final; Colour; Transition metal oxides; Hydrotalcites

1. Introduction

Layered double hydroxides (LDHs) with the hydrotalcite (HT)-like structure have deserved increasing interest in the last two decades. Their structure can be derived from that of brucite, $Mg(OH)_2$, formed by an hexagonal close-packing of hydroxyl anions, with Mg^{2+} cations occupying all octahedral sites in one out of two interlayers; a partial Mg^{2+}/Al^{3+} isomorphical substitution gives rise to a positive charge, which is balanced by intercalation of anions in the originally empty interlayers; these interlayers also host water molecules, with hydrogen bonding developing in the whole system (layer hydroxyls–water molecules–carbonate anions), in addition to the stronger electrostatic interactions between the positively charged layers and the interlayer anions. The formula of hydrotalcite, originally described from a mineral deposit in Snarum (Norway) in 1842, corresponds to $Mg_6Al_2(CO_3)(OH)_{16}{\cdot}4(H_2O)$, although it is generally written as $[Mg_{0.75}Al_{0.25}(OH)_2](CO_3)_{0.125}{\cdot}0.5(H_2O)$ to stress its relationship with brucite, $Mg(OH)_2$; the "formula" between the brackets corresponds to that of the layers, and the remaining to the interlayer. The Mg^{2+}/Al^{3+} molar ratio can take different values, but in those cases where it is lower than 2 electrostatic repulsion between adjacent octahedra containing Al^{3+} cations gives rise to weakened stability (and segregation of aluminum hydroxide), while for values larger than 5 formation of brucite is usually observed.

The interest in this compound has been enhanced because of several factors, namely: (i) compounds with the same structure, but with other cations in the layers and other anions in the interlayer, can be easily prepared (in addition to being found in nature); (ii) the interlayer species can be exchanged by an ion exchange process; (iii) on thermal decomposition, they yield highly dispersed mixed oxides with large specific surface area; (iv) other properties related to the specific nature of the existing chemical species (cations and anions). The properties have been reviewed by several authors,[1–9] and among the most outstanding properties, we can cite their use as catalysts or catalyst supports[1,10–12]; antacids and drug support for controlled delivery,[13] due to their basic properties,[14] anion scavenging for water purification,[15,16] composites,[17] etc. As mentioned above,

* Corresponding author. Tel.: +34 923 29 44 89; fax: +34 923 29 45 74.
E-mail address: vrives@usal.es (V. Rives).

0955-2219/$ – see front matter © 2011 Elsevier Ltd. All rights reserved.
doi:10.1016/j.jeurceramsoc.2011.11.033

the nature of the layer cations and the interlayer anions can be varied within given limits, but the M^{II}/M^{III} molar ratio and the ion size of the cations are two of the most relevant shortcomings, but many different cations have been incorporated in the brucite-like layers, although LDHs with lanthanide cations in the layers have been prepared.[18–21] In applications where homogeneous particle size distribution is important, or where high dispersion of the LDH particles is desirable, delamination,[22] or application of microwave treatment has demonstrated its high applicability.[23]

As thermal decomposition leads to highly dispersed mixed oxides,[24] coloured mixed oxides can be prepared when using solids with transition metal cations in the layers, their precise colour being tuned by the precise chemical composition of the LDH precursor, and thus these solids can be also used as precursors for ceramic pigments preparation.[25] We have previously reported on the use of different LDH precursors to prepare these ceramic pigments, but in all cases, rather strongly coloured solids were prepared. It is well known that obtaining a ceramic pigment with a definite colour is a difficult task, specially if pure black is pursued. Actually, the black pigments currently available for industry contain a rather large number of different cations, in order to obtain solids strongly absorbing in all the visible range. Here we report a facile method to prepare a black ceramic pigment by calcination of a LDH containing cobalt and chromium in the brucite-like layers. A detailed study to determine the optimum molar ratio between these two cations has been carried out and the pigment has been incorporated into two different commercial enamels.

On the other hand, the traditional method (solid state reaction) to obtain ceramic pigments requires a very high temperature and long calcination times, and it is also necessary to add flux agents to improve the reaction rate. With the method here proposed, we avoid the use of these flux agents, which generally are highly contaminant, and the temperature is decreased to 1200 °C for 2 h, instead of 1500 °C for 24 h, generally used in the ceramic industry.

2. Experimental

2.1. Samples preparation

All reagents were from Panreac (Spain), purism, and were used without any further purification.

The samples were prepared by slow addition of an aqueous solution containing Co^{2+} and Cr^{3+} in the established ratio, over a basic solution, at room temperature. The total volume was calculated for a 2 M total concentration of metal cations, and the volume of the basic solution was twice that of the metal cations solution. The amounts of reagents were calculated assuming that in the final product, whichever the cation molar ration, the solid had a LDH structure.

The metal cations solutions were prepared by slow, alternate, addition of $CoCl_2{\cdot}6H_2O$ (M = 237.71 g/mol) and $CrCl_3{\cdot}6H_2O$ (M = 266.45 g/mol) to distilled water at room temperature. Five samples were prepared with relative amounts of these salts corresponding to Co^{2+}/Cr^{3+} molar ratios of 2/1, 3/2, 1/1, 2/3 and 1/2. The solution was mechanically stirred during addition of the salts and this took between 90 and 120 min. The solutions were filtered, and no solid residue was isolated.

Similarly, the basic solution was prepared by addition of NaOH (M = 40 g/mol) and $NaHCO_3$ (M = 84.01 g/mol) to distilled water. The amount of $NaHCO_3$ was calculated for a $Cr^{3+}/CO_3{}^{2-}$ molar ratio of 1.0 in the final mixture, while the amount of NaOH was that necessary to neutralize $HCO_3{}^-$ anions and to obtain the hydrotalcite-like solid. Before mixing with the Co, Cr solution, the basic solution was left for 35–40 min to reach room temperature.

Formation of a greyish blue precipitate was observed from the very early stages of the addition of the metal cations solution to the basic one. Addition of the metal cations solution extended along 3–4 h while the suspension was being stirred at 600 ± 10 rpm using a model RZR = Z051 vertical stirrer from Heidolph. Once the addition was completed, stirring was maintained further for 20–24 h. The suspension was then filtered using a Buchner funnel (20 cm diameter) connected to a water pump. The filtered solutions were colourless and their pH was in the 8.5–9.5 range.

The solid was washed seven times with portions of 200 ml of distilled water; after addition of each portion the mixture was left in the funnel for 20–30 min before turning on the water pump. The washing liquids were also colourless. After completing the washing step, air was circulated through the cake for 2–3 h and then the solid was spread over glass plates for 4–5 days until it was dry; finally, the samples were hand ground in an agate mortar.

The samples will be named as CoCr0X, where X = 1, 2, 3, 4, and 5 stand for the solids with Co/Cr nominal ratios of 2/1, 3/2, 1/1, 2/3, and 1/2, respectively.

These solids were calcined in an oven at 1200 °C, at a heating rate of 5 °C/min and a retention time of 2 h; these calcined solids will be named as CoCr0X/1200. Some solids (named as CoCr0X/T) were calcined at intermediate temperatures (T in °C).

2.2. Techniques

Element chemical analysis for metal cations was carried out in Servicio General de Análisis Químico Aplicado (Universidad de Salamanca, Spain) by atomic absorption in a Mark-II ELL-240 apparatus after dissolving the samples in concentrated nitric acid.

Powder X-ray diffraction patterns were recorded in a Siemens D-500 diffractometer, using Cu Kα radiation (λ = 1.54050 Å) connected to a DACO-MP microprocessor; commercial Diffract-AT software was used. The tube power was 1200 W (40 kV and 30 mA) and the scanning rate was 0.5° (2θ)/min. The crystalline phases were identified by comparison with ASTM-JCPDS files and literature.

Differential thermal analysis (DTA) was carried out in a Perkin-Elmer DTA-7 instrument and the thermogravimetric analysis in a TGA 7-HT thermobalance, also from Perkin-Elmer, in both cases in flowing (30 ml/min) oxygen (99.995%, from L'Air Liquide, Spain). Both instruments were controlled by a

Table 1
Elemental chemical analysis data, thermogravimetric analysis data and specific surface areas of the samples prepared.

Sample	CoCr01	CoCr02	CoCr03	CoCr04	CoCr05
Element chemical analysis					
Co (%)	28.16	25.89	20.59	15.36	12.38
Cr (%)	12.34	15.33	18.05	20.54	21.54
Na (%)	0.81	1.17	1.4	2.45	3.85
C (%)	1.66	1.95	2.14	2.2	2.16
Co^{II}/Cr^{III} (molar ratio)	2.01	1.49	1.01	0.66	0.51
TG analysis data					
%Mass loss up to 200 °C	25.1	26.2	26.7	29.6	29.6
%Mass loss 200–400 °C	12.9	13.1	13.6	13.0	13.1
%Mass loss above 400 °C	3.4	2.1	2.1	2.5	2.5
Specific surface area (m^2/g)	24	39	48	54	59

PC via TAC 7/DX interfaces, and Pyris, Series Thermal Analysis System (version 3.0) software was used to analyse the raw data. The heating rate was in both cases 10 °C/min and the final temperature reached was 1000–1100 °C. Evolved gases were analysed with a Pfeiffer Vacuum mass spectrometry analyser.

Temperature programmed reduction (TPR) analysis were carried out in a TPR/TPD 2900 instrument from Micromeritics, equipped with a W–Au thermal conductivity detector, coupled to a Olivetti 300-28 data acquisition system. The reducing gas (also from L'Air Liquide) was a H_2/Ar mixture (5 vol%), with a flow of 60 ml/min, at a heating rate of 10 °C/min, up to 900 °C using ca. 50 mg of sample. These experimental conditions were chosen to avoid any sort of experimental artifacts.[26] Quantitative determination of consumed hydrogen was carried out by computer integration of the areas of the peaks, using reduction of CuO (from Merck) as a reference.

The FT-IR spectra were recorded in a M-1700 2B spectrometer from Perkin-Elmer, using commercial Spectrum V 2.00 software, in the 4000–400 cm^{-1} spectral region. The samples were prepared in KBr discs (ca. 1 mg sample/300 mg KBr), pressed at 10 T/cm^2. Forty scans were averaged, at a nominal resolution of 4 cm^{-1}, to improve the signal-to-noise ratio.

The UV–vis spectra were recorded in a Perkin-Elmer Lambda 35 spectrophotometer, using MgO as a reference.

The nitrogen adsorption–desorption isotherms at −196 °C were recorded in an automatic volumetric instrument from Micromeritics, model ASAP 2000. About 200 mg of sample was used, previously degassed in situ at 100 °C at residual pressure of 10^{-5} Torr for 5 h.

Particle size distribution analysis was carried out with a Malvern, model Mastersizer 2000 instrument, by laser radiation diffraction. The laser beam is directed towards a cell containing a dilute suspension of the solid in water, and dispersed in different angles, depending on the particle size. To favour dispersion and deaggregation of the particles, ultrasounds were also applied for 5 min, using the Hydro 2000 G accessory.

The colour of the samples was determined with a Konica Minolta colorimeter, model Chroma Meter CR 400, using a pulsed Xenon light. Data were stored in a computer connected to the colorimeter via a RS-232 interface and were treated using commercial software Colour Data CM-100W, Spectra Magic NG.

The $L^*a^*b^*$ colour space, designed by CIE and also known as CIE-Lab, has been used, where L^* stands for luminosity (0 for black and 100 for white), and a^* and b^* are chromaticity coordinates (positive and negative a^* for red and green, respectively, and positive and negative b^* for yellow and blue, respectively). Three measurements (three sparks each) were averaged for three different portions of each sample, which had been located between two transparent flat glasses within a black sample-holder. The instrument had been previously calibrated with a white reference (CR-A 43) from Minolta. Measurements were carried out for the bulk samples, and also after loading (2%, w/w) them on a white (WE) or a colourless (CE) enamel. The compositions of these enamels were MgO (3.7–3.8%), CaO (9.9–11.7%), Na_2O (3.6–3.7%), Al_2O_3 (21.1–21.2%), SiO_2 (51.6–55.5%) and B_2O_3 (4.2%), the difference being the presence of ZrO_2 (5.8%) in the white one. Once applied, the mixtures (pigment and enamel) were fired at 1140 °C for 50 min.

3. Results and discussion

3.1. Element chemical analysis

Samples showed a greyish blue colour, somewhat changing according to their precise chemical composition. Results for metals (Co and Cr; Na has been also analysed because of likely contamination from the basic solution) and C are included in Table 1. The values for the Co/Cr molar ratios for the different samples are also included in this table. The values are very close to those in the starting aqueous solutions and acceptable within experimental error. All samples also contain a small amount of sodium, which increases with the chromium content. This difference should arise from the different abilities of the solid phases forming on changing the Co/Cr ratio to retain adsorbed sodium species; as mentioned above, washing was repeated until a constant pH for the washing liquids was measured. Washing was not prolonged to avoid formation of HCO_3^-, instead of CO_3^{2-}, in the interlayer. The formulae calculated assuming a hydrotalcite structure formed by Co(II) and Cr(III) cations in the brucite-like layers are included in Table 2. On reporting these tables, we have assumed that the cations maintain their original formal oxidation states, and formation of the hydrotalcite-like structure (as confirmed by the PXRD data, see below), which molar

Table 2
Formula of the original samples prepared. The number of mole of the hydrotalcite phase or the Cr_2O_3 phase (see text), as well as the water content, are given per 100 g of sample.

Sample	$[Co_{0.668}Cr_{0.332}(OH)_2](CO_3)_{0.166}$	Cr_2O_3	H_2O (exp)	H_2O (t)
CoCr01	0.716	–	1.45	1.08
CoCr02	0.658	+0.038	1.40	0.99
CoCr03	0.523	+0.082	1.72	0.78
CoCr04	0.392	+0.132	1.94	0.59
CoCr05	0.315	+0.154	2.00	0.47

exp: experimental; t: theoretical.

fraction is limited by the Co^{2+} content, with a Co/Cr molar ratio of 2 (lower values have been proved to provide rather unstable hydrotalcite-like phases). The chromium in excess is formulated as the sesquioxide, Cr_2O_3. However, it should be remembered that when Cr^{3+} is precipitated as a hydrated oxide or hydroxide from aqueous solutions, it can be partially hydrolyzed, forming chromite species.[27] The number of mole for each phase corresponds to a total mass of solid of 100 g. As shown in Table 2, as the chromium content increases, the molar fraction of Cr_2O_3 (or a related phase) increases. The experimental water content has been calculated from the TG curves (see below), while the theoretical water content (last column in Table 2) corresponds to the maximum amount of water which can be located between the hydrotalcite layers, close packing them with the interlayer carbonate anions. Obviously, as the molar fraction of the hydrotalcite-like phase decreases (on passing from sample CoCr01 to sample CoCr05), the amount of water to be located between the layers decreases. However, the experimental water content increases, showing that it should be mostly related to the other phase existing in these samples.

As shown in Table 1, the C content also increases steadily with the Cr content; as in this same sense the molar fraction of the hydrotalcite decreases, the increasing amount of carbon (which runs parallel to the increase in Na content) can be tentatively assigned to formation of increasing amounts of sodium carbonate (or hydrogencarbonate) which has not been removed on washing.

3.2. Powder X-ray diffraction and specific surface area

The diagrams for all five samples are included in Fig. 1. Crystallinity (as concluded from the sharpness of the maxima) is not too high, and decreases from sample CoCr01 to sample CoCr05, as the Cr content is increased.

The main diffraction lines recorded for the Cr-poor samples (namely, samples CoCr01 and CoCr02) coincide with those reported for hydrotalcite, $Mg_6Al_2(CO_3)(OH)_{16}\cdot 4H_2O$ (JCPDS file 14-0191) and reevesite, $Ni_6Fe_2(CO_3)(OH)_{16}\cdot 4H_2O$ (JCPDS file 20-0786). As the Cr content is increased, these maxima become hardly detectable, especially in the low diffraction angle range, and new maxima develop, which can be ascribed to the presence of hydrated chromium hydroxide, $Cr(OH)_3\cdot 3H_2O$ (JCPDS file 03-0864) and grimaldiite, CrO(OH) (JCPDS file 9-0331). In the last three diagrams, the presence of the maxima due to diffraction by basal planes of the hydrotalcite-like phase, close to 10 and 20° (2θ), is only concluded from the presence of broad reflections in the expected range. However, the maximum close to $2\theta = 60°$ seems to be still present.

The specific surface areas for the original samples are also given in Table 1. A steady increase from 24 m^2/g for sample CoCr01 to 59 m^2/g for sample CoCr05 is observed. These changes should be related to development of the additional phase, in addition to the hydrotalcite one, as the chromium content is increased; the mostly amorphous nature of this phase would account for the specific surface area increase.

3.3. Thermal analysis

The thermogravimetric (TG) curves for the starting compounds prepared are included in Fig. 2. The curves are similar to each other in all five cases, and several steps can be identified in all cases. The differential curves (DTG), also included in this figure, permit to identify the temperature ranges at which these changes occur. The DTG curves show that the first mass loss (ca. 27% as an average value) has been completed around 200 °C, and so this temperature has been taken as the end-point of the first process. The second one extends up to ca. 400 °C and above this temperature only a smooth mass loss is observed in all cases. It should be noticed, however, that the minima of the DTG curves in the first step slightly shift towards lower temperature when the Cr^{3+} content is increased, and two different behaviours can be observed: (i) samples CoCr01 and CoCr02, and (ii) the other

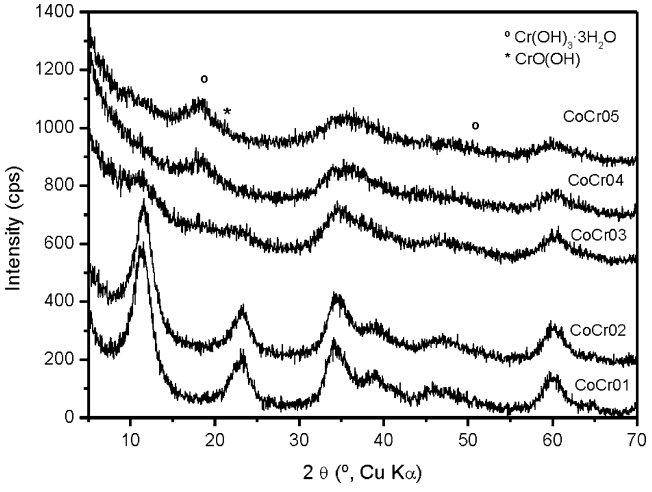

Fig. 1. Powder X-ray diffraction diagrams for the original samples prepared. The diagrams have been vertically displaced for clarity.

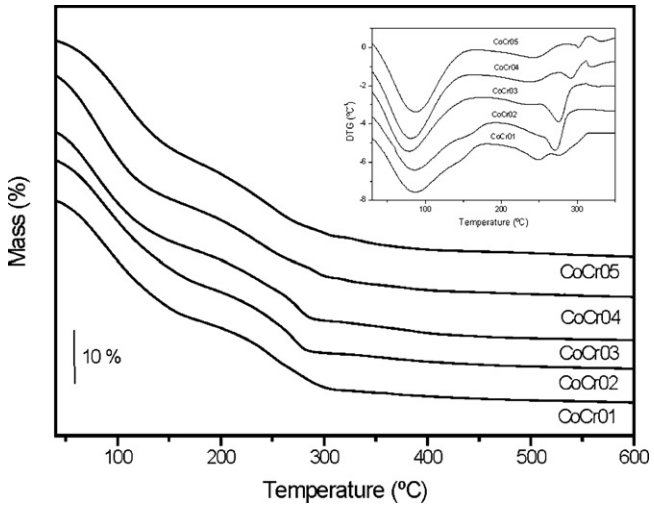

Fig. 2. Thermogravimetric curves for the five original samples. The inset shows the corresponding derivative curves. In both cases the curves have been vertically displaced for clarity.

three samples. Mass spectrometric analysis of the gases evolved indicates that only water vapour is released in this temperature range, probably weakly adsorbed on the external surface of the particles, as well as from the interlayer space of the crystals. The shift of the DTG minima towards lower temperatures as the chromium content is increased indicates that water removal is easier in these last three cases, a behaviour that should be undoubtedly related to the lower LDH molar fraction, and the larger molar fraction of the hydrated Cr^{3+} hydroxide phase in the last three samples, from which water release will be easier. From a quantitative point of view, a smooth increase in the mass lost up to 200 °C is observed; the values are summarised in Table 1.

The second step has been taken from 200 to 400 °C, where all the effects seem to have been completed, as an almost flat horizontal line is recorded above this temperature in the DTG curves (range not shown). These curves show one or two weaker effects around 260–300 °C, which seem to be independent on the precise chemical composition of the solids. The mass loss (average value ca. 13%) is nearly constant for all five samples, and it is also markedly lower than in the first step. The evolved gases were water vapour and carbon dioxide, from decomposition of the interlayer carbonate species. If we assume that the molar fraction of the LDH phase in the initial solid is limited by the amount of Co^{2+} ions, then the increase in mass loss cannot be attributed to an increase in the molar fraction of the LDH phase, which would lead to larger amounts of CO_2 and H_2O being released, but to the presence of Cr^{3+} oxohydroxides, which dehydration would be responsible for this effect. The results of mass spectrometry analysis are in agreement with previous studies with a Mg, Al LDH[28]; these data confirm the absence of residual chloride anions in the interlayer.

The mass loss above 400 °C corresponds only to 2–3% of the initial mass of sample; the TG curves show an almost undetectable slope, and this is usually ascribed to removal of residual hydroxyl groups as water vapour or strongly held carbonate species.

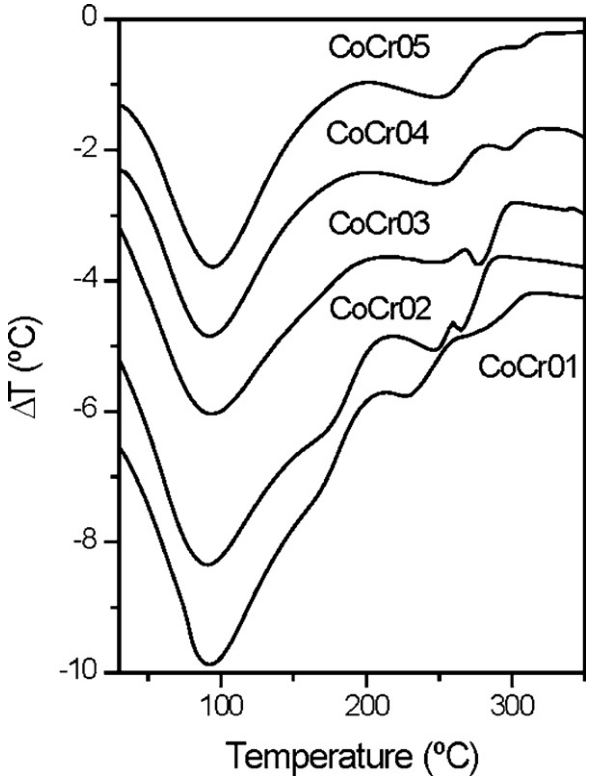

Fig. 3. Differential thermal analysis curves for the five original samples. The diagrams have been vertically displaced for clarity.

Summarising, mass loss takes place in three main steps, from room temperature to 200, from 200 to 400 and from 400 °C upwards. In addition, differences can be also found depending on the Co/Cr molar ratio. These processes have been quantified from the TG data and analysis of the solid residues for samples CoCr01 and CoCr05, as both wings of the composition span.

The DTA curves for all five samples are included in Fig. 3. The shapes of the curves are rather similar, from a qualitative point of view, to the DTG curves, shown in Fig. 2. This is not unexpected, as all phenomena occuring in the temperature range shown correspond to endothermic mass losses. There is a strong endothermic effect around 100 °C, shifting to lower temperature as the chromium content is increased, due to water removal, and which shift is related to the lower energy required to remove water for the Cr-rich samples. The weaker effects between 200 and 300 °C should be related to removal of carbon dioxide and water vapour.

The PXRD patterns of the solids calcined at 1200 °C (CoCr0X/1200) are included in Fig. 4. The most relevant maxima correspond to a spinel phase, with weaker maxima corresponding to other species. Despite calcinations at lower temperature (500 °C) seems to be enough to produce the spinel phase, we have chosen to study the phases formed after calcinations at 1200 °C because dispersion of the pigment in an enamel matrix requires temperatures around 1140 °C, as these phases will be those existing after the high temperature calcinations.

Previous studies[29,30] have shown that calcination of Co^{2+}-containing LDHs in air or in nitrogen leads to an oxidation (at least partially) of Co^{2+} to Co^{3+} species, and thus, several

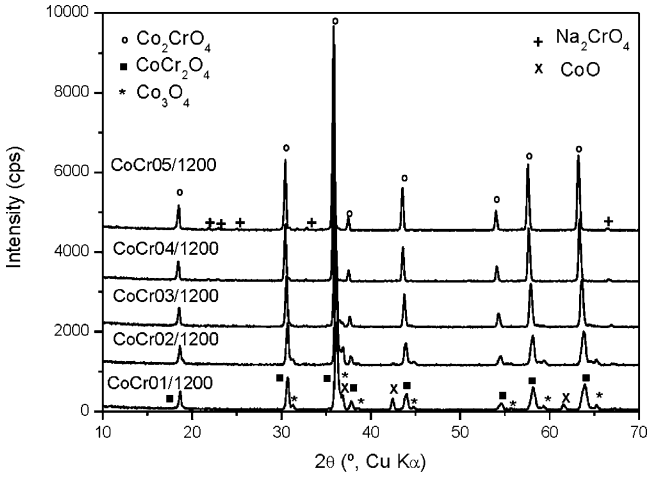

Fig. 4. Powder X-ray diffraction diagrams for the samples calcined at 1200 °C. The diagrams have been vertically displaced for clarity.

compounds with the spinel phase can be formed in our samples, namely: Co_3O_4, Co_2CrO_4, and $CoCr_2O_4$, or even mixed phases. The PXRD data for these compounds are collected in the JCPDS database, and this will help to identify the residues formed upon high temperature calcination of our samples. The main diffraction maximum corresponds to planes (3 1 1), and it is recorded at 2.438, 2.460, and 2.512 Å, respectively, for Co_3O_4, Co_2CrO_4, and $CoCr_2O_4$ (files 09-0418, 24-0326, and 20-1084, respectively). In our samples its position shifts smoothly from 2.480 Å (sample CoCr01/1200) to 2.504 Å (sample CoCr05/1200). This means that as the chromium content is increased, the position of the main maximum of the spinel phase also shifts, and thus a change in the chemical composition of the spinel phase should be concluded.

The sharpness of the maxima increases also in the same direction. In addition to the diffraction maxima of the spinel phase, other maxima are also recorded. Some weak ones correspond to the rock-salt structure of CoO, which are recorded for the calcined Cr-poor samples, and disappear for the Cr-rich samples. We have previously shown[30] that calcination of CoCr LDHs at very high temperatures leads to a partial decomposition of the spinel phase, forming the rock-salt type CoO. The presence of Na_2CrO_4, specially in sample CoCr05/1200, can be also tentatively suggested, although it seems to exist as well for some of the other samples; formation of Na_2CrO_4 has been definitively concluded (see below).

Formation of Co_3O_4 is only observed in the two chromium-poor samples, but only as a minor component to the other spinel phases. Formation of the other two spinels (i.e., Co_2CrO_4 and $CoCr_2O_4$) could be tentatively suggested; their molar fraction would depend on the Co/Cr molar ratio in the initial, un-calcined compound. So, for sample CoCr01/1200, with a Co/Cr molar ratio equal to 2, Co_2CrO_4 (where both Co^{2+} and Co^{3+} species coexist together with Cr^{3+}) is the major component, while for sample CoCr05/1200, with a Co/Cr molar ratio equal to 0.5, the major (even exclusive) component should be $CoCr_2O_4$. This conclusion is also supported from the position of the diffraction line due to planes (3 1 1), recorded at 2.480 Å for sample CoCr01/1200 (the value was 2.46 Å for Co_2CrO_4) and at 2.504 Å for sample CoCr05/1200 (2.512 Å for the $CoCr_2O_4$ spinel). Segregation of CoO in sample CoCr01/1200, as suggested by the PXRD data, would probably account for a minor content of $CoCr_2O_4$ and the shift to 2.48 Å of the (3 1 1) signal for sample CoCr01/1200.

The PXRD diagrams of the samples have been also recorded after heating at different temperatures along the heating treatment. For instance, data for sample CoCr03 (Co/Cr molar ratio equal to 1) calcined at 500, 750, 1000, and 1200 °C are included in Fig. 5A. As it can be seen in this figure, formation of the spinel phase is already evident upon calcination at 500 °C, although the maxima are rather broad. As the calcination temperature is increased, the peaks become sharper, but their positions do not change, indicating that the phases existing at the highest calcination temperature reached by our equipment (1200 °C) are already formed even at 500 °C, after collapsing of the layered structure, although they are less crystalline.

Together with the maxima of the spinel phase, these diffractograms show also some very weak signals which have been tentatively ascribed to the presence of Na_2CrO_4, specially in sample CoCr05 (not shown). To check formation of this compound upon calcination, we have taken samples CoCr03/T (T = 500, 750, 1000, and 1200 °C) and have washed them with distilled water; then we have recorded the PXRD diagrams of the washed solids, as well as that of the solid precipitated from the washing liquids upon evaporation of water. The PXRD diagrams of the washed solids are included in Fig. 5B. As it can be clearly seen in this figure, the maxima due to the spinel phase remain unaltered, but the very weak signals have completely disappeared, indicating that they are due to a water-soluble compound. The PXRD diagram of the solid isolated upon evaporation of the washing water is included in Fig. 5C, and it coincides with that reported in the JCPDS file (22-1365) for Na_2CrO_4, thus definitively confirming formation of Na_2CrO_4 during calcination of our Cr-rich samples. A further confirmation of formation of this compound comes from the FT-IR of the washed and un-washed residues calcined at 500 or 1000 °C (Fig. 5D); the weak bands around 950–850 cm^{-1} due to mode ν_3 of CrO_4^{2-} species, clearly recorded for the unwashed solid, are absolutely absent after washing them with distilled water.

3.4. Temperature-programmed reduction

The curves recorded for all five precursors are shown in Fig. 6. As it can there be seen, reduction starts in all cases above 350 °C and the general intensity of the curve decreases, with the absolute maximum shifting towards higher temperatures, as the chromium content is increased.

Starting from sample CoCr01, it shows an intense reduction effect centered around 430 °C (which might be composed of several overlapped effects, see below), followed by a very weak effect at ca. 600 °C. A similar curve, but with less intense effects, shifted towards higher temperatures, is recorded for sample CoCr02, and in this case the first effect is clearly a composed

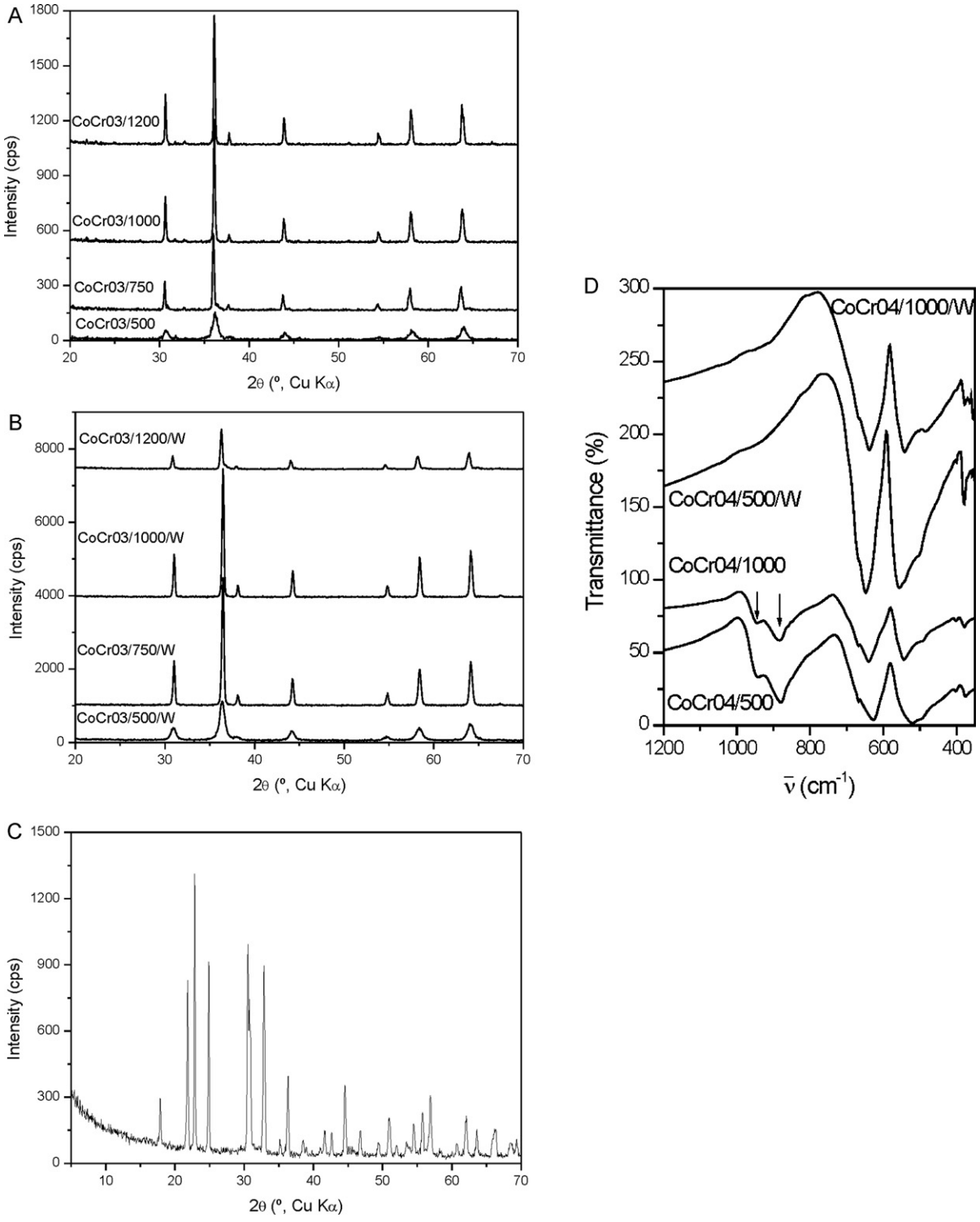

Fig. 5. (A) Powder X-ray diffraction diagrams for sample CoCr03 calcined at different temperatures (given in °C). The diagrams have been vertically displaced for clarity. (B) Powder X-ray diffraction diagrams for sample CoCr03 calcined at different temperatures and washed with distilled water. The diagrams have been vertically displaced for clarity. (C) Powder X-ray diffraction diagram of the solid isolated from the washing liquids. (D) FT-IR spectra of sample CoCr04 calcined at 500 and 1000 °C and washed (/W) after the thermal treatment. The arrows indicate the bands typical of sodium chromate. The spectra have been vertically displaced for clarity.

one. The two Cr-rich samples show only a two-components effect, with maxima around 450 and 520 °C, and the high temperature one has vanished. Sample CoCr03 shows an intermediate behaviour. Probably, the most noticeable feature is the decrease of the area under the curve recorded (it should be mentioned that almost the same amount of sample, 37–38 mg, were used in all cases), which is directly related to the amount of hydrogen consumed during reduction. Such a decrease spans from 88

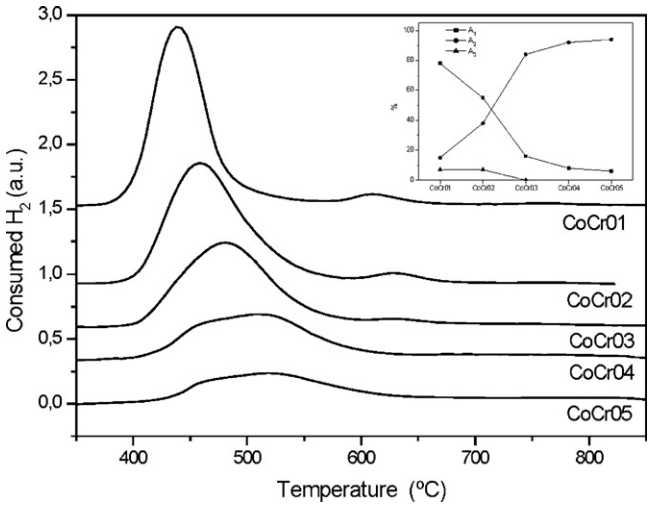

Fig. 6. Temperature-programmed reduction curves for the five original samples. The inset shows the relative areas of the components after deconvolution. The diagrams have been vertically displaced for clarity.

for sample CoCr01 to 56 for sample CoCr03 and 30 for sample CoCr05 (in arbitrary units).

According to the literature,[31,32] Cr^{3+} species are not reduced under the experimental conditions here used, while Co-containing species are reduced to the zero-valent state. Consequently, if the cations maintain their original oxidation state, we have assumed that the reaction taking place during the TPR experiments is

$$Co^{2+} + H_2 \rightarrow Co^0 + 2H^+$$

The ratio between the amount of hydrogen experimentally consumed and that requested for total reduction of Co(II) to Co(0) is in all cases very close to unity, deviations being not larger than 12%, rather reasonable bearing in mind the experimental procedure used. Only for sample CoCr05 the amount consumed is 23% larger than the expected one for the exclusive presence of Co(II), suggesting that a partial oxidation to Co(III) now being reduced has taken place during preparation of this sample.

In all cases the main maximum seems to be a composed one, suggesting that reduction takes place in several steps or different reducible species exist in these samples.

We have carried out a deconvolution of these curves, keeping the number of maxima to the minimum value to reach a reasonably good fit. Three components were needed for samples CoCr01 and CoCr02 (although the weight of component 3 was scarcely 7%), but a good fit was achieved with two components only for the other three samples. The first maximum was recorded at 438–465 °C for all five samples (the precise position steadily shifting towards higher temperatures as the chromium content was increased), while the second component was recorded at 607–625 °C for samples CoCr01, CoCr02, and CoCr03, but at 701–723 °C for the other two samples.

The change in the relative intensities of these component maxima is shown in Fig. 6(inset). The relative intensity for the first reduction effect decreases when the molar fraction of chromium is increased, especially from sample CoCr03 upwards, the second maximum amounting almost 100% of the total reduction process for samples CoCr04 and CoCr05.

These results clearly suggest the presence of species with different reducibility. A first approach could be to assume the presence of Co(III) species, which are reduced at low temperatures to Co(II), and that the second maximum corresponds to total reduction to the zero-valent state. However, this is not the case, as the quantitative analysis of hydrogen consumption does not support this assumption: the exclusive presence of Co(II) would give rise to a value of 1.00 for the ratio between the measured and the calculated (for Co(II) reduction) amounts of hydrogen consumed, while the exclusive presence of Co(III) would give rise to a value of 1.5, with relative intensities of the first and second maxima of 1:2, and this is not the case for any sample. Even the presence of cobalt in both oxidation states would not fit with the experimental relative values of the component maxima, at least for samples CoCr01 and CoCr02. If 50% oxidation of Co^{2+} species to Co^{3+} ones has taken place, the ratio between the experimental and the theoretical amounts of hydrogen consumed would be 1.25, nicely coinciding with the value calculated for sample CoCr05, but we do not think this is the case. First of all, we should not ignore the presence of Na_2CrO_4, as concluded from the PXRD and FTIR results discussed above; in addition, the Co_2CrO_4 phase, found by PXRD for sample CoCr05/1200, has been formed upon extremely oxidant (oxygen reach) conditions; under TPR experimental conditions the oxidant agent could be the interlayer carbonate species or even the chromate impurity. Consequently, we cannot insight further in the meaning of the quantitative TPR analysis.

As the amount of chromium increases the molar fraction of the low crystalline phase also increases (Fig. 1), as well as the relative intensity of the second reduction maxima in the TPR curves (Fig. 6). So we can conclude that the first reduction maximum should mostly correspond to reduction of Co^{2+} from the hydrotalcite-like phase.

3.5. Fourier-transform infrared spectroscopy

The spectra recorded for all five samples are included in Fig. 7. The broad, asymmetric absorption band centered around 3450 cm^{-1} is due to the stretching mode of OH groups. This band, as noted before,[33,34] is very broad, because of the presence of hydroxyl groups in different environments and, consequently, different energy situations, namely, as water molecules, as layer hydroxyl groups, and with hydrogen bonding with the interlayer carbonate anions. Moreover, the phases identified in addition to the hydrotalcite-like one also correspond to hydroxyl-containing ones.[35] The band is very asymmetric, with an evident shoulder slightly below 3000 cm^{-1}, probably clearer for sample CoCr01, which has been ascribed[24,36,37] to the stretching mode of hydroxyl groups which are hydrogen-bonded to interlayer carbonate anions. The shoulder is less intense as the chromium content is increased, in agreement with the lower molar fraction of the hydrotalcite phase in the Cr-rich samples.

The bands recorded from 3000 to 1000 cm^{-1}, in addition to the "energy absorptions" around 2300 cm^{-1} due to a miscancellation of the bands due to atmospheric CO_2, are mostly due to

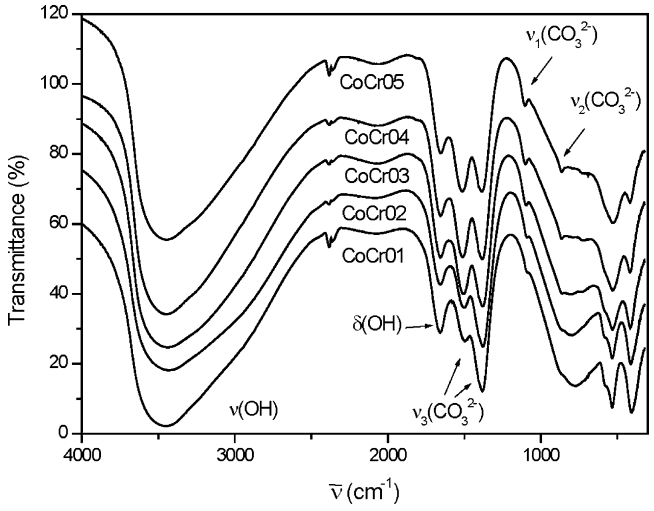

Fig. 7. FT-IR spectra of all five original samples. The spectra have been vertically displaced for clarity.

the interlayer species. The first one (from high wavenumbers) at 1645 cm^{-1} is due to the bending mode of water molecules, which are located both in the interlayer and as hydration, probably, of the non-hydrotalcite co-phases. The other bands are due to carbonate species. The band due to mode ν_3 of this anion (T_2 symmetry in point group D_{3h}) is infrared active, and is recorded around 1430 cm^{-1}.[38] For our samples, two bands are recorded close to this position, namely, one at 1482 ± 5 cm^{-1} and another one at 1360 ± 5 cm^{-1}, suggesting a decrease in the local symmetry of the carbonate anion and the corresponding (at least partial) loss of degeneracy of this vibrational mode. Such a symmetry decrease could be related to formation of hydrogen bonds with interlayer water molecules. It should be also noticed that the relative intensities of these two bands do not remain constant for all samples. Of course, it is rather difficult to decide whether the intensity of one band decreases or the intensity of the other increases. However, we should notice that the band due to the stretching mode of hydroxyl groups remains roughly with the same intensity in all five spectra, as well as that due to the bending mode of water molecules at 1645 cm^{-1}. The intensity of the band at 1360 ± 5 cm^{-1} remains also almost constant, and so we conclude that the actual behaviour observed corresponds to an increase in the relative intensity of the band at 1482 ± 5 cm^{-1} as the chromium content is increased.

It should be noticed that the decrease in symmetry of the carbonate anion from D_{3h} to C_{2v} activates mode ν_1, originally forbidden in IR, which is recorded as a very weak absorption at 1070 ± 10 cm^{-1}. The intensity of this peak slightly increases also with the chromium content.

Finally, the bands recorded below 1000 cm^{-1} are due to lattice vibrations of the brucite-like layers, except the weak band at 840 cm^{-1}, due to mode ν_2 of carbonate, which is clearly recorded when the intensity of the broad band around 756 cm^{-1} decreases as the chromium content is increased. Below this position, two bands are recorded at 508 ± 3 cm^{-1} and 390 ± 5 cm^{-1}, which relative intensities change with the chromium content too. On comparing with the band at 1360 ± 5 cm^{-1}, due to interlayer carbonate species, we can conclude that the intensity of the band at 508 ± 3 cm^{-1} is roughly constant in all five spectra, and the effect observed as the chromium content is increase is a progressive weakening of the band at 390 ± 5 cm^{-1}. On comparing the changes in intensities with the chromium content from sample CoCr01 to CoCr05, we should conclude that bands at 756 and 390 ± 5 cm^{-1} should be related to vibrations involving cobalt cations, as their intensities decrease as the molar fraction of cobalt decreases in this series of samples. The vibrations involve M–O or M–O–M moieties in the structure of the layers.

3.6. Visible–ultraviolet spectroscopy

The spectra for the five original samples are included in Fig. 8. The bands are recorded in very close positions in the different spectra, although a change in their relative intensities can be easily observed, as well as a small shift in their precise positions.

According to the results above commented and discussed, both cations, cobalt and chromium, are located in octahedral holes in the brucite-like structure (in addition to the Cr-containing extra phase), and consequently the bands recorded should correspond to Laporte-forbidden, spin-allowed transitions. From the TPR result we conclude that the oxidation state of the cations in the original samples are Cr(III) and (almost exclusively) Co(II). According to the literature,[39] *d–d* transitions involving [$Co^{III}O_6$] species are spin-forbidden and so their intensities should be extremely low. Those involving [$Co^{II}O_6$] species, despite spin-allowed, are very weak, as they correspond to the simultaneous excitation of two electrons. On the contrary, those bands originated by transitions involving [CrO_6] species will be much stronger and will dominate the spectra. Two bands

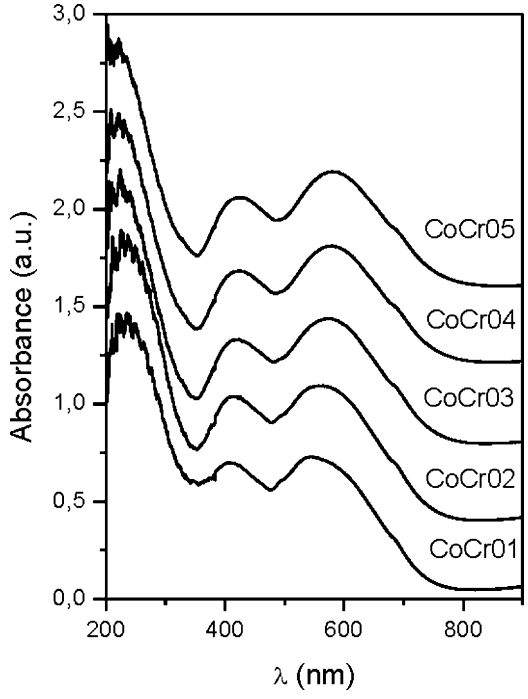

Fig. 8. Vis–UV spectra of all five original samples. The spectra have been vertically displaced for clarity.

Table 3
Ascription and position (nm) of the bands recorded in the vis–UV spectra of the samples prepared. The values calculated for the crystal field splitting energy ($10Dq_0$, cm^{-1}), the Racah parameter (B, cm^{-1}), the nephelauxetic parameter (β) and the expected position for band ν_3 (cm^{-1}) are also given.

Band	Ascription	CoCr01	CoCr02	CoCr03	CoCr04	CoCr05
ν_1	$^4A_{2g}(F) \rightarrow {}^4T_{1g}(F)$	545	560	571	576	581
ν_2	$^4A_{2g}(F) \rightarrow {}^4T_{2g}(F)$	408	415	420	422	425
ν_4	$^4A_{2g}(F) \rightarrow {}^2E_g$	680	680	680	680	680
$10Dq_0$		18,350	17,860	17,510	17,360	17,210
B		588	601	610	617	616
β		0.64	0.65	0.66	0.67	0.67
ν_3	$^4A_{2g}(F) \rightarrow {}^4T_{1g}(P)$	39,360	38,490	37,880	37,640	37,340

are recorded in the visible range, and the *band* recorded between 200 and 300 nm should be ignored, as it is overlapped with charge-transfer processes and in addition the response of the diffuse reflectance detector in this high energy range is rather low and almost unreliable (see the noise in the spectra). Consequently, our discussion will be based exclusively on the two bands recorded in the visible range.

The first band, at 545–581 nm, shifts towards larger wavelengths and enhances as the chromium content is increased (see Table 3), and it corresponds to the spin-allowed $^4A_{2g}(F) \rightarrow {}^4T_{1g}(F)$ transition. The second band is recorded at 408–425 nm, also shifting towards larger wavelength and weakening as the chromium content is increased. It is due to the $^4A_{2g}(F) \rightarrow {}^4T_{2g}(F)$ transition.

From the equations reported by Dou[40] the crystal field splitting energy and the Racah parameter for all five samples have been calculated (Table 3), and from these values, the position of the third band has been calculated, Table 3. The Racah parameter (values also given in Table 3) also increases with the chromium content, thus giving a nephelauxetic parameter indicating a strong ionic character for the Cr–O bond. All these values (positions of the bands, CFSE, B and β) increase with the chromium content in the series studied. This can be due to the decrease in the molar fraction of the hydrotalcite-like phase and the increase in that of chromium oxo- and hydroxides as the chromium content is increased.

All spectra show, in addition, a very weak shoulder close to 680 nm (its precise position can not be determined with more accuracy because of its weakness, on the high wavelength side of the more intense band close to 560 nm), which might correspond to the so-called "rubi band", a spin forbidden $^4A_{2g}(F) \rightarrow {}^2E_g$ transition.[41]

The changes observed in the relative intensities of the bands deserve a further comment. It is obvious, from the PXRD data above, that on passing from sample CoCr01 to sample CoCr05, the molar fraction of the hydrotalcite-like phase decreases; in the same sense, the intensity and broadness of the high wavelength band increases and the spectra are overall shifted towards larger wavelengths. We should conclude that this shift ought to be associated to the increasing content in chromium oxohydroxides in the samples. No major change is however observed because Cr^{3+} is under an octahedral coordination in all the solids which have been identified by PXRD.

Due to their almost completely black colour, the solids calcined at high temperature show vis–UV spectra consisting of an almost horizontal line at high absorbance values, which makes extremely difficult to identify the component bands.

3.7. Particle size distribution

The particle size distribution was originally rather broad, but decreased upon ultrasounds treatment; in other words, such a "large" particle size for the untreated solids should be taken as an artifact; consequently, we will only discuss on the ultrasound-treated samples. The distribution was rather symmetric in all cases, although as the chromium content was increased a weak shoulder for lower particle size develops for the 1200 °C calcined samples. Regarding the uncalcined solids, the average particle size was around 30 μm in all cases, decreasing to 20 μm for the calcined samples. These results suggest that the method use is rather appropriate to prepare solids with an homogeneous particle size distribution, and that no sintering occurs upon high temperature calcination.

3.8. Colour coordinates

As the aim of this study is to prepare and to characterise ceramic pigments which are treated at high temperatures, the samples calcined at 1200 °C as described above have been also studied. So, we have determined the colour coordinates of the original solids, the solids calcined at 1200 °C and both sets of solids applied to white (WE) and colourless (CE) enamel, with 2% (w/w) pigment loading. The study has been also extended to samples CoCr03 and CoCr04 calcined at increasing temperatures, without application of enamels.

Luminosity (L^*) results for all samples studied are included in Fig. 9A. As expected, luminosity increases for the enamel supported samples, obviously when the white enamel was used. As calcination of the samples leads to almost black solids, luminosity for the bulk calcined solids shows values below 5. The enamel-supported samples prepared with the previously calcined samples also show L^* values slightly lower than for those samples where the original (uncalcined) sample was incorporated to the enamel. For a given treatment

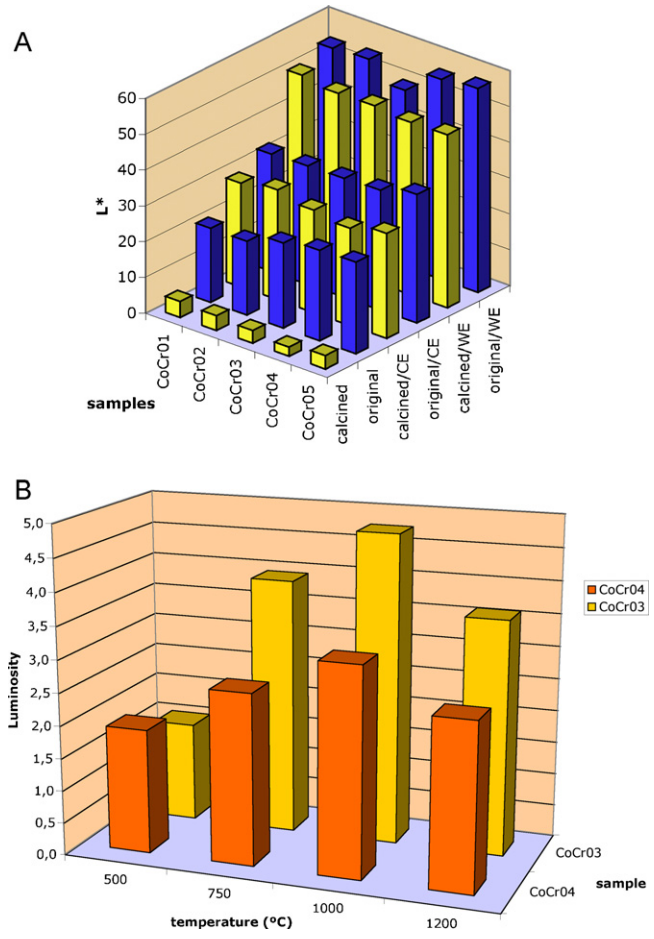

Fig. 9. (A) Change in luminosity of the samples: original ones, calcined at 1200 °C, dispersed in white (WE) or colourless (CE) enamel and submitted to calcination at 1140 °C. The dispersed pigment had not (original/CE or original/WE) or had been (calcined/CE or calcined/WE) calcined at 1200 °C prior to be dispersed in the enamel. (B) Change in luminosity of samples CoCr03 and CoCr04 with the calcination temperature.

and a given enamel support, the values of L^* do not differ significantly from one sample to another, although roughly speaking, it decreases as the chromium content increases for the calcined samples, but slightly increases for the uncalcined samples.

Concerning samples CoCr03 and CoCr04 calcined at different temperatures, luminosity is always lower than 5, but showing a maximum when the solids were calcined at 1000 °C, Fig. 9B.

Colour coordinates a^* and b^* were also measured. It should be stressed that to the naked human eye, all calcined samples appeared black, but quantitative determination of parameters a^* and b^* showed some slight, but important, differences. Concerning the quality of a black pigment, the closer to zero the values of a^* and b^*, the higher the quality of the pigment. The results are shown in Fig. 10, where values of coordinates a^* and b^* have been plotted for each series of samples.

Concerning the bulk solids calcined at 1200 °C, Fig. 10A, both a^* and b^* approach to zero for samples CoCr03 and CoCr04, this last being somewhat better than the first one. It means that if one is interested in a black power, should prepare sample CoCr04 and calcine it at 1200 °C in air. However, this is not applicable in industry, where an enamel will be used.

It should be pointed out that the presence of small amounts of Na_2CrO_4 in some of the samples has a negligible effect on their colour coordinates, probably because it has a light yellow colour and has no effect when mixed with the almost completely black colour of the calcined solids.

The plots for the solids containing the white enamel (WE) and calcined at 1140 °C, but containing original, Fig. 10B, or previously calcined solids, Fig. 10C, show that in no case a reliable black solid is obtained. The best compromise is obtained for sample CoCr05 if starting from the uncalcined solid, Fig. 10B, although both a^* and b^* showing negative values, bluish or greenish colours would be expected. Similar results are observed when the solid previously calcined at 1200 °C is incorporated to the white enamel, Fig. 10C; in this case the compromise for both low a^* and b^* values is also obtained for a composition between those of samples CoCr04 and CoCr05, but in this case the absolute values for the coordinates are larger than in the former case, and thus more intense green-blue colour is expected.

Promising results are, however, obtained with the colourless enamel (CE). In this case, the closest to zero values of a^* and b^* are obtained for a composition between those of samples CoCr03 and CoCr04 (both values being between 0 and −0.5), Fig. 10D, while values of −1 are measured when the pigment has not been previously calcined at 1200 °C, Fig. 10E, for a chemical composition between those for pigments CoCr02 and CoCr03.

Concerning the effect of the calcination temperature, values of a^* and b^* between 0 and −0.4 (i.e., very close to absolute black) are obtained for sample CoCr03 calcined at 750 °C or above, Fig. 10F.

Bearing in mind that the particle size is almost the same in all cases, we should conclude that these compositions, around that corresponding to sample CoCr03, are optimal for preparation of a black ceramic pigment. From a technological point of view, the slightly worse a^* and b^* values for the systems prepared with original pigment (but merely values of −1 instead of −0.5) could be overcome by the fact that in this system only a calcination step, once the pigment has been mixed with the colourless enamel, is needed.

Finally, comparison of the $L^*a^*b^*$ parameters of our pigments with those of two commercial pigments (A and B) has shown the good quality of ours and consequently the suitability of the preparation procedure here described. These two pigments, when dispersed in a colourless enamel showed values of $L^* = 35.55$, $a^* = -0.32$ and $b^* = 3.50$ for sample A and $L^* = 32.27$, $a^* = -1.73$ and $b^* = 1.87$ for sample B. None of our pigments dispersed in the CE enamel (well previously calcined or uncalcined) shows L^* values larger than 30 (see Fig. 9A), indicating that our samples are darker than the commercial ones. Concerning the a^* and b^* parameters, those for our samples (CoCr03 and CoCr04, see Fig. 10D) are closer to zero than those for the commercial ones, while they are of the same order when the original, uncalcined sample is dispersed in the colourless enamel (Fig. 10E).

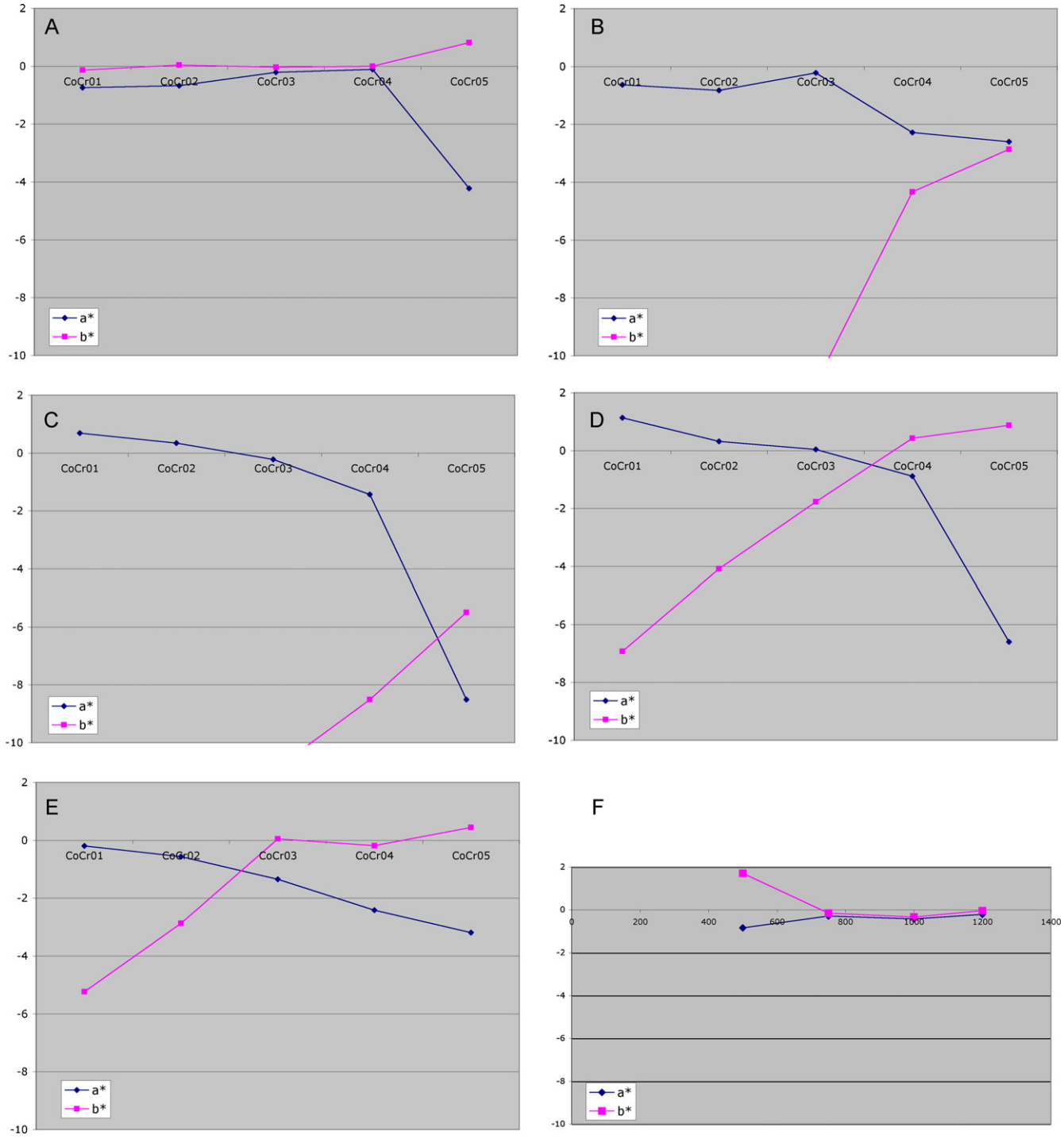

Fig. 10. (A) Change in colorimetric parameters a^* and b^* for all samples calcined at 1200 °C. (B) Change in colorimetric parameters a^* and b^* for the original samples dispersed in a white enamel and calcined at 1140 °C. (C) Change in colorimetric parameters a^* and b^* for the samples calcined at 1200 °C, dispersed in a white enamel and calcined at 1140 °C. (D) Change in colorimetric parameters a^* and b^* for the samples calcined at 1200 °C, dispersed in a colourless enamel and calcined at 1140 °C. (E) Change in colorimetric parameters a^* and b^* for the original samples dispersed in a colourless enamel and calcined at 1140 °C. (F) Change in colorimetric parameters a^* and b^* for sample CoCr03 calcined at different temperatures.

4. Conclusions

A simple method has been developed to prepare a true black ceramic pigment from calcined non-stoichiometric hydrotalcites. The chemical composition (molar Co/Cr) fraction determines the colour of the final solid, together with the calcination temperature and the precise nature of the enamel used. In this way, depending on the specific use to be given to the pigment (as a bulk, or in white or colourless enamel), a given chemical composition and a precise calcination temperature should be chosen. The colours developed by some selected samples are of better quality, as concluded from the $L^*a^*b^*$

parameters, than two commercial black pigments, tested under the same experimental conditions.

Acknowledgments

Authors thank financial support from ERDF, MICINN (grant MAT2009-08526) and Junta de Castilla y León (grant SA111A09). Thanks are given to Mr. A. Montero for his assistance in obtaining some of the experimental results.

References

1. Cavani F, Trifirò F, Vaccari A. Hydrotalcite-type anionic clays: preparation, properties and applications. *Catal Today* 1991;**11**:173–301.
2. Trifirò F, Vaccari A. Hydrotalcite-like anionic clays (layered double hydroxides). In: Atwood JED, Davies JL, MacNicol DD, Vögtle F, Lehn J-M, editors. *Comprehensive supramolecular chemistry*. Oxford: Pergamon; 1996. p. 251–91.
3. Vaccari A. Preparation and catalytic properties of cationic and anionic clays. *Catal Today* 1998;**41**:53–71.
4. Rives V, Ulibarri MA. Layered double hydroxides (LDH) intercalated with metal coordination compounds and oxometalates. *Coord Chem Rev* 1999;**181**:61–120.
5. Rives V, editor. *Layered double hydroxides: present and future*. New York: Nova Sci Pub Inc; 2001.
6. Wypych F, Satyanarayana KG, editors. *Clay surfaces: fundamentals and applications*. Amsterdam: Elsevier; 2004.
7. Rives V. Characterization of layered double hydroxides and of their decomposition products. *Mater Chem Phys* 2002;**75**:19–25.
8. Duan X, Evans DG, editors. *Layered double hydroxides*. Berlin: Springer; 2006.
9. Bergaya F, Theng BKG, Lagaly G, editors. *Handbook of clay science*. Amsterdam: Elsevier; 2006.
10. Basile F, Vaccari A. Applications of hydrotalcite-type anionic clays (layered double hydroxides) in catalysis. In: Rives V, editor. *Layered double hydroxides: present and future*. New York: Nova Sci Pub Inc; 2001. p. 285–321.
11. Monzón A, Romeo E, Marchi AJ. Hydrogenation catalysis by mixed oxides prepared from LDH. In: Rives V, editor. *Layered double hydroxides: present and future*. New York: Nova Sci Pub Inc; 2001. p. 323–82.
12. Rives V, Carriazo D, Martín C. Heterogeneous catalysis by polyoxometalate-intercalated layered double hydroxides. In: Gil A, Korili SA, Trujillano R, Vicente MA, editors. *Pillared clays and related catalysts*. New York: Springer; 2010. p. 319–97.
13. Costantino U, Nocchetti M. Layered double hydroxides and their intercalation compounds in photochemistry and in medicinal chemistry. In: Rives V, editor. *Layered double hydroxides: present and future*. New York: Nova Sci Pub Inc; 2001. p. 383–411.
14. Del Arco M, Martín C, Martín I, Rives V, Trujillano R. A FT-IR spectroscopic study of surface acidity and basicity of mixed Mg,Al-oxides obtained by thermal decomposition of hydrotalcite. *Spectrochim Acta (A)* 1993;**49A**:1575–82.
15. Ulibarri MA, Hermosín MC. Layered double hydroxides in water decontamination. In: Rives V, editor. *Layered double hydroxides: present and future*. New York: Nova Sci Pub Inc; 2001. p. 251–84.
16. Goh K-H, Lim T-T, Dong Z. Application of layered double hydroxides for removal of oxyanions: a review. *Water Res* 2008;**42**:1343–68.
17. Taviot-Gueho C, Leroux F. In situ polymerization and intercalation of polymers in layered double hydroxides. In: Duan X, Evans DG, editors. *Layered double hydroxides*. Berlin: Springer; 2006. p. 121–59.
18. Fernández JM, Barriga C, Ulibarri MA, Labajos FM, Rives V. New hydrotalcite-like compounds containing yttrium. *Chem Mater* 1997;**9**:312–8.
19. Gunawan P, Xu R. Lanthanide-doped layered double hydroxides intercalated with sensitizing anions: efficient energy transfer between host and guest layers. *J Phys Chem C* 2009;**113**:17206–14.
20. Musimeci AW, Xu ZP, Smith SV, Minchin RF, Martin DJ. Layered double hydroxide nanoparticles incorporating terbium: applicability as a fluorescent probe and morphology modifier. *J Nanopart Res* 2010;**12**:111–20.
21. Domínguez M, Pérez-Bernal ME, Ruano-Casero RJ, Barriga C, Rives V, Ferreira RAS, et al. Multiwavelength luminescence in lanthanide-doped hydrocalumite and mayenite. *Chem Mater* 2011;**23**:1993–2004.
22. Jaubertie C, Holgado MJ, San Roman MS, Rives V. Structural characterisation and delamination of lactate-intercalated Zn,Al-layered double hydroxides. *Chem Mater* 2006;**18**:3114–21.
23. Benito P, Labajos FM, Rives V. Microwaves and layered double hydroxides: a smooth understanding. *Pure Appl Chem* 2009;**81**:1459–71.
24. Labajos FM, Rives V, Ulibarri MA. Effect of hydrothermal and thermal treatments on the physicochemical properties of Mg–Al hydrotalcite-like materials. *J Mater Sci* 1992;**27**:1546–52.
25. Nebot-Díaz I. PhD thesis, Universitat Jaume I, Castelló (Spain); 2001.
26. Malet P, Caballero A. The selection of experimental conditions in temperature programmed reduction experiments. *JCS Faraday Trans I* 1988;**84**:2369–75.
27. Greenwood NN, Earnshaw A. *Chemistry of the elements*. 2nd ed. Oxford: Butterworth Heinemann; 1998.
28. Rives V. Comment on "Direct observation of a metastable solid phase of $Mg/Al/CO_3$-layered double hydroxide by means of high temperature in situ Powder XRD and DTA/TG". *Inorg Chem* 1999;**38**:406–7.
29. Del Arco M, Galiano MVG, Rives V, Trujillano R, Malet P. Preparation and study of decavanadate-pillared hydrotalcite-like anionic clays containing cobalt and chromium. *Inorg Chem* 1996;**35**:6362–72.
30. Del Arco M, Rives V, Trujillano R. Cobalt-iron hydroxycarbonates and their evolution to mixed oxides with the spinel structure. *J Mater Chem* 1998;**8**:761–7.
31. Rives V, Ulibarri MA, Montero A. Application of temperature-programmed reduction to the characterization of anionic clays. *Appl Clay Sci* 1995;**10**:83–93.
32. Labajos FM, Rives V. Thermal evolution of Cr(III) ions in hydrotalcite-like compounds. *Inorg Chem* 1996;**35**:5313–8.
33. Kloprogge JT, Frost RL. Infrared and Raman spectroscopic studies of layered double hydroxides (LDHs). In: Rives V, editor. *Layered double hydroxides: present and future*. New York: Nova Sci Pub Inc; 2001. p. 139–92.
34. Kloprogge JT. Infrared and Raman spectroscopy of naturally occurring hydrotalcites and their synthetic equivalents. In: Kloprogge JT, editor. *The application of vibrational spectroscopy to clay minerals and layered double hydroxides*. Aurora, CO: The Clay Mineral Society; 2005. p. 204–38.
35. Nakamoto K. *Infrared and Raman spectra of inorganic and coordination compounds*. Hoboken: John Wiley & Sons; 2009.
36. Ross GJ, Kodama H. Properties of a synthetic magnesium-aluminum carbonate hydroxide and its relationship to magnesium-aluminum double hydroxide manasseite and hydrotalcite. *Am Mineral* 1967;**52**:1036–7.
37. Stanimirova TS, Vergilov I, Kirov G, Petrova N. Thermal decomposition products of hydrotalcite-like compounds: low-temperature metaphases. *J Mater Sci* 1999;**34**:4153–61.
38. Hisatsume IC, Adl T, Beahm EC, Kempf RJ. Matrix isolation and decay kinetics of carbon dioxide and carbonate anion free radicals. *J Phys Chem* 1970;**74**:3225–31.
39. Sutton D. *Electronic spectra of transition metal complexes*. Maidenhead: McGraw-Hill Pub Co Ltd; 1968.
40. Dou YS. Equations for calculating Dq and B. *J Chem Educ* 1990;**67**:134.
41. Jørgensen CK. Spectroscopy of transition-group complexes. *Adv Chem Phys* 1963;**5**:33–146.